

## RESEARCH ARTICLE

# ERT Based Computation of Solid Phase Fraction in Solid-Liquid Flow With Various Object Sizes

YONGGUANG TAN<sup>ID</sup>, SHIHONG YUE<sup>ID</sup>, ZIQIANG CUI<sup>ID</sup>, (Member, IEEE),  
AND HUAXIANG WANG<sup>ID</sup>, (Senior Member, IEEE)

School of Electrical Automation and Information Engineering, Tianjin University, Tianjin 300072, China

Corresponding author: Shihong Yue (shyue1999@tju.edu.cn)

This work was supported by NSFC under Grant 61973232.

**ABSTRACT** Solid phase fraction (*SPF*) is one of the most important parameters in solid-liquid two-phase flow, and has been increasingly addressed on most of the measuring techniques. As an effective measuring technique, Electrical Resistance Tomography (*ERT*) has been applied to measure *SPF* owing to low-cost, fast-response, non-invasive and non-radiation characteristics. The *ERT*-based *SPF* estimation is greatly affected by different solid object sizes from the existing methods, but currently there is none efficient method to solve this problem. In this paper, a mathematical model firstly is proposed to generally approximate various object sizes and thereby reconstruct all measurements. Therefore, when all solid objects have unevenly distributed and different sizes, *SPF* can still be effectively computed. Experiments are implemented in three groups of actual experiments by a building platform, where the solid objects in each group have individual object size. Results show that the new method can compute the value of *SPF* more accurate than the existing method, and thus provide a more accurate way to *SPF* computation.

**INDEX TERMS** Measurement reconstruction, solid phase fraction, object size, *ERT*.

## I. INTRODUCTION

Solid-liquid two-phase flow is widely encountered in process industry [1], and solid phase fraction (*SPF*) estimation in flow pipe plays an important role in process detection and parameter analysis. The high precision of *SPF* is necessarily required to effectively control and optimize industrial processes. Despite *SPF* was studied using various tomographic modalities, such as a single source  $\gamma$ -ray computed tomography [2], ultrasonically-based detection techniques [3] etc. But as a valuable imaging technique, electrical resistance tomography (*ERT*) [4] provides both the cross-sectional image and the *SPF* value in solid-liquid two-phase flow in a detected pipe. Compared with other tomographic techniques, *ERT* is a fast, low-cost, and nondestructive technique in obtaining 2D/3D distribution parameter information [5].

The *ERT*-based phase fraction estimation methods have evolved for many years, and each progress provides information of better accuracy and stronger robustness [6]. Various

estimation methods can be categorized to hardware reformulation and algorithm progress. Our research in this paper focuses on the latter. Almost all the *SPF* estimation algorithms result from the Maxwell-Garnett (*MG*) formula [7], but its preliminary form is very inaccurate due to inevitable assumptions and complex application conditions. For example, for the solid-liquid two-phase flow in dredging engineering [8], the *MG* formula remains rather inaccurate. Generally, there are the following three problems at least:

1) Solid and liquid objects are assumedly small-size and evenly distributed, and thereby *SPF* can be computed by the *MG* equation. But actual sizes generally are various [9], and thereby the computed value of *SPF* may be very inaccurate.

2) Most the existing methods focus on the gas-liquid two-phase flow whose natural characteristics are different from those of the solid-liquid two-phase flow. And the conductivity difference between gas and liquid is much larger than that between solid and liquid inclusions. Meanwhile, gas is compressible but solid is not, leading different *SPFs*.

3) The *ERT* image is of low spatial resolution by which the small objects are not found at all [10]. Meanwhile, there

The associate editor coordinating the review of this manuscript and approving it for publication was Mansoor Ahmed<sup>ID</sup>.

are inevitable noises and random artifacts in an ERT image. However, the accuracy of MG formula is assured only if the object size is small enough, which is contradictive to the ability of ERT spatial resolution.

In the past decades, efforts have been made to overcome the above problems. Numerical simulations have been present for phase volume fraction of solid-liquid multiphase flows in horizontal pipe [11]. To raise measurable range of phase fraction, various void fractions has been tested [12], and the void fraction was estimated based on the polynomial regression of measurement voltage values. Recent research [13] shows that if the sensitivity matrix in the ERT process is carefully determined, the phase fraction estimation can be improved by integrating the prior information in practice. More related reviews can be found in [14]. However, these studies don't involve the solid object sizes and distributions, and thus cannot effectively and accurately find correct SPF in the solid-liquid two-phase flow. Specially, the above three problems may coexist, and leads to the estimated SPF by MG unbelievable. Consequently, it is an emergency task to develop feasible and accurate SPF estimation method to overcome the above problems.

In this paper, a mathematical model firstly is used to estimate the solid object size, and then thereby ERT measurements are reconstructed and the MG formula is extended to a new form associated with various object sizes. Finally, the proposed method is validated under a group of actual experiments with typical characteristics.

## II. RELATED WORK

The section includes two parts: ERT measuring principle and MG formula.

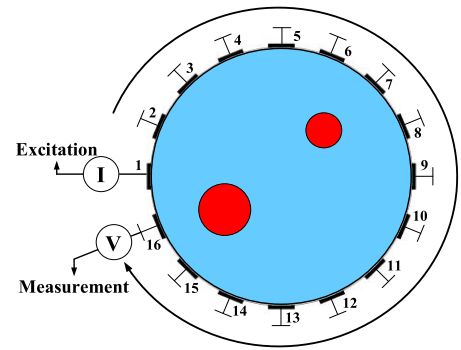
### A. ERT MEASURING PRINCIPLE

We use a typical 16-electrode ERT system to explain the ERT measuring principle. ERT measures the flow parameter in a field  $\Omega$  by boundary measurements [15].

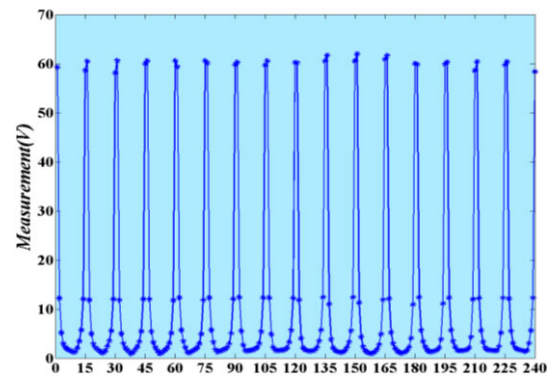
Fig. 1(a) shows the ERT measuring process in  $\Omega$ . First, an exciting current "I" is added to the electrode 1, and 15 measurements are obtained in other 15 electrodes; then "I" is added to the electrode 2, and 15 measurements are obtained again. The process is repeated in turns till all 16 electrodes are excited. Therefore, total 240 measurements are obtained to compute the parameters in  $\Omega$ . These 240 measurements construct 16 "U" shape curves in which each responds to the same excitation, as shown in Fig.1 (b).

The ERT measuring process obeys the general Maxwell equation [16]. Let  $\partial\Omega$  be the boundary domain of  $\Omega$ . The boundary measurement  $u$  in  $\partial\Omega$ , the electrical potential  $\phi$ , and conductivity  $\sigma$  inside  $\Omega$  satisfy

$$\begin{cases} \nabla \cdot (\sigma \nabla \phi) = 0, & \text{in } \Omega \\ \text{s.t., } \begin{cases} \int_{\partial\Omega} \sigma \cdot \frac{\partial \phi}{\partial n} ds = I, & \text{on exciting electrode at } \partial\Omega \\ \phi = u, & \text{on measuring electrode at } \partial\Omega \end{cases} \end{cases} \quad (1)$$



(a) Excitation and measurement of ERT



(b) 16 U-shape curves from 240 measurements

FIGURE 1. The measuring process of ERT and all measurements from 16 electrodes.

where  $I$  is the exciting current. The ERT process is tightly close to the inverse problem of the Dirichlet boundary conditions [17], which solves  $\sigma$  in  $\Omega$  by all boundary value  $u$ .

The actual measurement in  $\Omega$  is required to use a reference field  $\Omega_0$  in which all pixels have the same conductivity value [18]. After individually exciting  $\Omega_0$  and  $\Omega$ , the increments of both  $\sigma$  and  $u$  in the two fields are  $\Delta\sigma$  and  $\Delta u$ , and (1) is further expressed as

$$\Delta u = J \Delta \sigma + O((\Delta \sigma)^2) \quad (2)$$

where  $J$  is a nonlinear relation from  $\Delta\sigma$  to  $\Delta u$ . Based on finite element method, the linearized and discrete form after neglecting nonlinear item of (2) can be expressed as the following equations,

$$\Delta U = S \Delta \sigma \quad (3)$$

where  $\sigma \in R^{n \times 1}$  is the vector of  $\sigma$ ,  $\Delta U \in R^{m \times 1}$  is the vector of measurements,  $S \in R^{m \times n}$  is called as sensitivity matrix in ERT as well,  $n$  is the number of pixels in  $\Omega$ , and  $m$  is the number of measurements. For a 16-electride system,  $m = 240$ ;  $n$  is typically taken as 812 due to only 240 measurements available. When both  $\Delta U$  and  $S$  are known, to solve  $\sigma$  can be used to compute all parameters in  $\Omega$ .

However, the directly analytic solution for (3) does not exist since the ERT inverse problem is both nonlinear and ill-posed. Many algorithms have been proposed to indirectly

solve the above ill-posed problem. The two most used algorithms are Linear Back Projection (*LBP*) [19] and Tikhonov regularization (*TR*) [20]. *LBP* has the highest time resolution, while in most applications *TR* has highest spatial resolution among all *ERT* algorithms if its parameter is optimally chosen. *LBP* solves the unknown  $\Delta\sigma$  in (3) by the following form,

$$\Delta\sigma = S^T \Delta U \quad (4)$$

Alternatively, *TR* is presented as a following minimization function as

$$Z = \|\Delta U - S\Delta\sigma\| + \mu R(\Delta\sigma) \quad (5)$$

where  $\mu$  is the regularization parameter and controls the tradeoff between the fidelity term  $\|\Delta U - S\Delta\sigma\|$  and the penalty term  $R(\Delta\sigma)$ . When  $R(\cdot)$  is take as an unit matrix, the one-step analytic solution of (5) is

$$\sigma = (S^T S + \mu I)^{-1} S^T U \quad (6)$$

So far, the two algorithms have widely applied in most cases of *ET* computation process. But the hyperparameter  $\mu$  in *TR* is difficult to be determined due to dynamical and various measuring process in application such as the dredging engineering etc [21], [22]. Hence, we only use *LBP* to the *ERT* process in this paper.

### B. MG EQUATION

*ERT* has used for the parameter detection of multiple-phase flow, and essentially the computation of dispersed phase fraction. Maxwell-Garnett (*MG*) formula [7] is the most used way to compute SPF  $\kappa$  in solid-liquid two-phase flow, it is

$$\kappa = \frac{2\sigma_1 + \sigma_2 - 2\sigma_{mc} - \sigma_{mc}\sigma_2/\sigma_1}{\sigma_{mc} - \sigma_{mc}\sigma_2/\sigma_1 + 2(\sigma_1 - \sigma_2)} \quad (7)$$

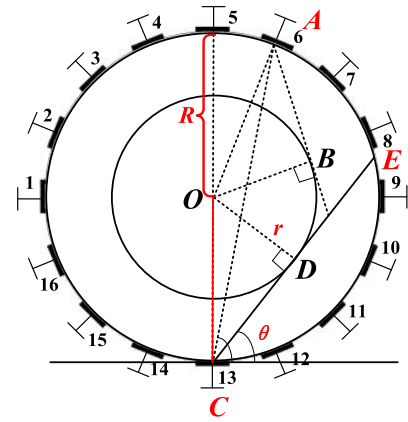
where  $\sigma_1$  is the conductivity of liquid-phase objects (e.g., seawater),  $\sigma_2$  is the conductivity of the detected solid-phase objects (e.g., soil or sand),  $\sigma_{mc}$  is the averaging conductivity of mixtures of solid- phase and liquid- phase objects. In case of non-conductive solid-phase objects,  $\sigma_2(k)$  is nearly 0 *s/m* and (7) is reduced as

$$\kappa = 6/(2 + \sigma_{mc}/\sigma_1) - 2 \quad (8)$$

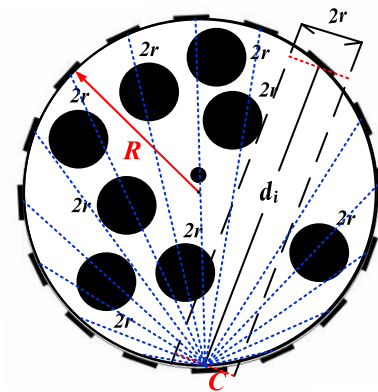
Equation (8) shows that the rate of  $\sigma_{mc}/\sigma_1$  becomes the only variable to compute the value of  $\kappa$ . Since both values of  $s_{ij}$  and  $u_i$  are known in any *ERT* process, thus *SPF* can be estimated.

Usually, the reference field  $\Omega_0$  in *MG* is directly taken as the conductivity of liquid- phase objects  $\sigma_1$  which is known in prior, for example,  $\sigma_1 = 32.5 \text{ uS/m}$  in seawater, while  $\sigma_1 = 0 \text{ s/m}$  in fresh water; Therefore,  $\kappa$  is uniquely determined by  $\sigma_{mc}$ . When applying *LBP*, there is the linear relation [23] between  $\sigma_{mc}/\sigma_1$  and  $\Delta U$ ,

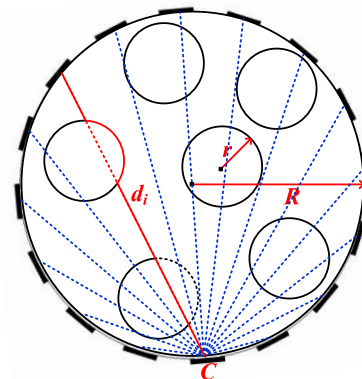
$$\sigma_{mc}/\sigma_1 = a \sum_{j=1}^{812} \sum_{i=1}^{240} s_{ij} \Delta u_i + b \quad (9)$$



(a) A large circle



(b) Intersected line and circles



(c) The shortest distance (in red)

FIGURE 2. Computation of effect of object size.

where  $a$  and  $b$  are two regression parameters to reconstruct  $\sigma_{mc}$  from  $\Delta\sigma$ . Therefore, after taking (9) to (8), it is

$$\kappa = 6/(2 + a \sum_{j=1}^{812} \sum_{i=1}^{240} s_{ij} \Delta u_i + b) - 2 \quad (10)$$

However, (10) is irrelative to solid object size in solid-liquid two-phase flow due to the following reasons:

1) There is none way to effectively express solid object shapes and sizes. In most applications, these objects may have

various sizes and uneven distributions which coexist in the same solid-liquid two-phase flow.

2) The mechanism is unknown that various object size affects *ERT* measurement. Even though there is an effective way to express the effect of object size to measurement, how to apply it to improve the accuracy of *SPF* is unknown as well.

3) The use of  $\sigma_{mc}$  to compute *SPF* in *MG* in fact assumes that solid object size is infinitesimal, but the spatial resolution is very limited. The actual size in *ERT* is impossible more than the size of pixels. Therefore, the assumption in *MG* doesn't hold.

4) The real  $\sigma_{mc}$  cannot directly be computed by *LBP* or other *ERT* algorithms, and for various values of  $\sigma_1$ , (9) must be regressed by available historical measurements. Otherwise, the value of *MG* cannot effectively be solved.

In this paper, we propose a mathematical model to express object size and object shape, and further solve the above three problems in a theoretical and practical way. Since object size and distribution in any cross-section in pipe is random and fast changing, thus they cannot be fixed in practice. Therefore, in our proposed method, object size and distribution are approximated in the sense of averaging value, and all the measurements are reconstructed in  $\Omega$ . Consequently, the estimated value of *SPF* is more accurate and reasonable than that of *MG*.

### III. THE PROPOSED METHOD

The proposed method is illustrated by two parts: analytic approximation of various object sizes and distributions, and the computation of *SPF* in two-phase flow.

#### A. APPROXIMATION OF OBJECT SIZE AND DISTRIBUTION

Let a detected *ERT* field  $\Omega$  with 16 electrodes be a circle with radius  $R$  (see Fig. 2(a)). According to the *Ohm law* [24], any measurement (potential difference) is approximately determined by two variables: the shortest distance from exciting to measuring electrodes and the area that is covered by currents. Since each exciting current goes through the same field  $\Omega$ , thus any measurement is determined by their shortest distance. In this following, we simulate the change of object size from a large circle to a set of small circles.

Assume that the object is a large circle  $\odot O$  that is located in the center of the field  $\Omega$  with radius  $r$  (see Fig.2 (a)). From an exciting electrode  $C$  to a measuring electrode  $E$ , their connection line  $CE$  has angle  $\theta$  to the horizontal line.

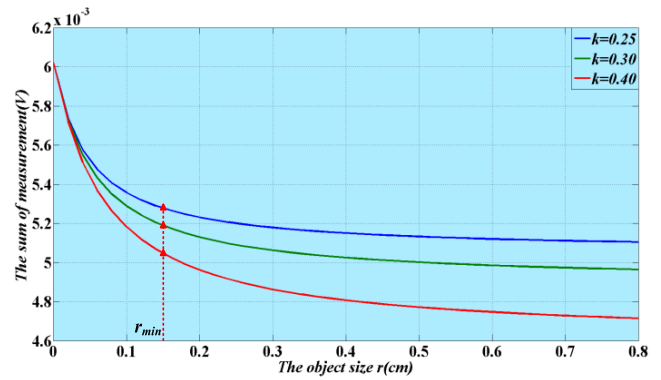
If  $CE$  is not intersected to  $\odot O$ , the measurement at  $E$  can nearly be computed as

$$\varphi_E = I/(4\pi\gamma d_E) \tag{11}$$

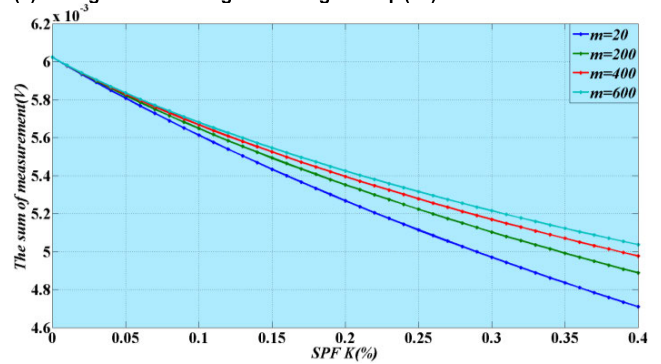
where  $I$  is the exciting current intensity,  $\gamma$  is the conductivity in  $\Omega$ , and  $d_E$  is equal to the length of segment  $CE$ .

Otherwise, if  $CE$  is intersected to  $\odot O$ ,  $d_E$  from  $C$  to  $E$  is computed as

$$d_E = AB + CD + \text{arc}(BD) = 2(\sqrt{R^2 + r^2} - \arcsin(r/R) + r\theta) \tag{12}$$



(a) Change of measuring sum along  $r$  in Eq. (18)



(b) Change of measuring sum along  $\kappa$  in Eq.(19)

FIGURE 3. The changing tendency of the measuring sum as  $r$  or  $\kappa$  is changed.

The value of  $\varphi_E$  can still be computed after taking (12) into (11), but it is smaller since  $d_E$  has an increment and becomes larger than the length of  $CE$ .

Generally, if all objects are  $m$  randomly distributed circles with the same radius  $r$  in  $\Omega$  (see Fig.2 (b)),  $\varphi_1, \varphi_2, \dots, \varphi_{15}$  are 15 relative measurements from the same excitation  $C$  to 15 other measuring electrodes. They have individual segments lengths from  $C$  to 15 measuring electrodes,  $d_1, d_2, \dots, d_{15}$ , respectively.

Note that the 15 segments at  $C$  are intersected to  $m$  circles in  $\Omega$  at a certain probability. In terms of width  $2r$ , the covering area of  $i$ th segment in  $\Omega$  nearly is  $2rd_i$  (see Fig. 2(b)), and thus the probability that anyone of  $m$  circles intersects to the line is  $2rd_i/(\pi R^2)$ . Hence, the number that all  $m$  circles intersects to the  $i$ th segment probabilistically is

$$2mrd_i/\pi R^2 \triangleq N_i, \quad i = 1, 2, \dots, 15 \tag{13}$$

In practice, the following problems must be considered:

1) These actual circle sizes usually are neither identical nor circle-shaped, but it is impossible to construct an accurate model to approximate these sizes and shapes.

2) Anyone of the  $m$  circles intersects 15 segments have different lengths. If the segment of the  $i$ th measurement is not intersected to any circle,  $d_i$  is equal to the segment length. Otherwise, for  $d_i$ , the shortest distance from  $C$  to  $i$ th



TABLE 1. The measuring sum under various values of  $r$ .

$\kappa$	Small objects	Middle objects	Large objects	Curve on $r$
0.25				
0.30				
0.40				

Note:  $\gamma=32.5uS/cm$ ; objects in blue.

TABLE 2. The solved range of  $q$  under various  $\gamma$  and  $K$ .

$\gamma(uS/cm) \setminus \kappa(\%)$	5	10	15	20
$\gamma=32.51$	[0.960,0.981]/0.102	[0.952,0.971]/0.108	[0.934,0.973]/0.127	[0.925,0.973]/0.113
$\gamma=18.52$	[0.912,0.979]/0.118	[0.932,0.989]/0.094	[0.929,0.968]/0.116	[0.918,0.942]/0.126
$\gamma=0.055$	[0.881,0.923]/0.182	[0.828,0.993]/0.085	[0.921,0.953]/0.109	[0.907,0.935]/0.105

Note: “\*/\*” is the range of  $q$  and the relative error of resultant measurements in the range, respectively.

measuring electrode must have an increment whose largest value is  $(\pi - 2)r$ , as shown in Fig.2(c).

For the first problem, we assume that the effect of various sizes and different shapes in measurements can still be approximated by  $m$  circles with the same size  $r$ . Nevertheless, any segment will intersect to  $N_i$  small circles according to (12). Consequently, for the second problem, assume that the increment of  $d_i$  relative to  $N_i$  intersecting circles obey a decreasing geometric series with common ratio  $q$ , and whereby the  $N_i$  increments on  $d_i$  are  $(\pi - 2)r, (\pi - 2)r q^1, \dots, (\pi - 2)r q^{N_i - 1}$ . Their sum is

$$s_i = (\pi - 2)r(1 - q^{N_i}) / (1 - q), \text{ s.t., } 0 < q < 1, \quad (14)$$

So the shortest distance of  $i$ th measurement is added to  $(d_i + s_i)$ ,  $\varphi_i$  in (11) is turned to

$$\varphi_i = \frac{I}{4\pi\gamma\{d_i + (\pi - 2)r(1 - q^{N_i}) / (1 - q)\}}, \quad i = 1, 2, \dots, 15 \quad (15)$$

Equation (15) originally recovers the interrelation between measurement and object (circle) size. To observe the effect of object size, we fix  $\kappa$  when objects are  $m$  circles, it is

$$m\pi r^2 / (\pi R^2) = \kappa \Rightarrow m = \kappa R^2 / r^2 \quad (16)$$

Taking (16) into (13), it is

$$N_i = 2\kappa d_i / (\pi r), \quad i = 1, 2, \dots, 15 \quad (17)$$

Equation (15) becomes

$$\varphi_i = \frac{I}{4\pi\gamma\{d_i + (\pi - 2)r(1 - q^{2\kappa d_i / (\pi r)}) / (1 - q)\}}, \quad i = 1, 2, \dots, 15 \quad (18)$$

Therefore, 15 measurements can be computed when all objects are evenly and randomly distributed in  $\Omega$ . Equation (18) shows that each measurement  $\varphi_i$  is a nonlinearly decreasing function on object size  $r$ , whereas the measurement in the MG formula is not related to  $r$ , leading to inaccurate estimation of  $\kappa$ .

Note that the sum of all measurements can reflect their global changing tendency. As  $r$  increases from 0 to  $R$  in  $\Omega$  but the value of  $\kappa$  is fixed individually at three different values, Fig.3 (a) shows the three curves of measuring sum from (18).

Note that it is impossible that  $r$  tends to an infinitely small value due to the limitation of pixel size. For example, the typical number of pixels in  $\Omega$  is 812, and thereby the minimal pixel size  $r_{min}$  is  $\pi R^2$  by 812. Fig. 3(a) shows that  $r_{min}$  is much larger than zero, and the measuring sum decreases globally as  $r$  increases.




Alternatively, according to (16), (18) is rewritten along  $\kappa$  to

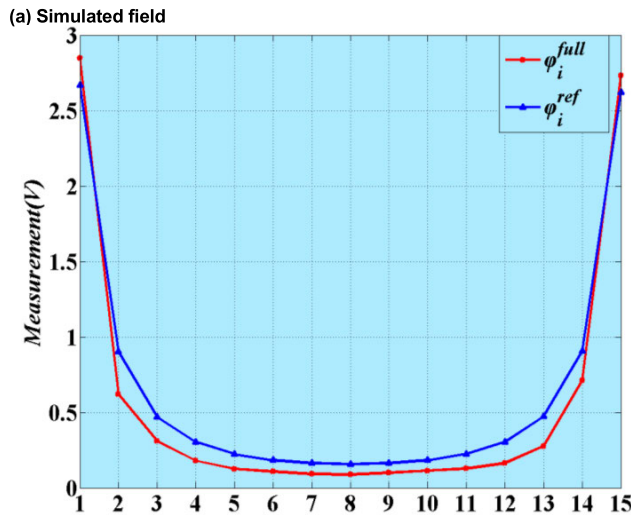
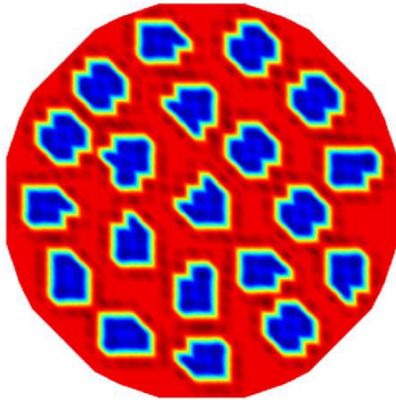
$$\varphi_i = \frac{1}{4\pi\gamma\{d_i + (\pi - 2)R\sqrt{\kappa/m}(1 - q^{2d_i\sqrt{\kappa m}/(\pi R)}) / (1 - q)\}} \quad (19)$$

Equation (19) shows that each measurement is determined by  $m$  and  $\kappa$  after  $r$  is fixed. But  $m$  is far larger than  $\kappa$ , thus  $m$  plays a key role in the computing measurement. As  $\kappa$  increases but  $m$  is fixed individually at four different values, Fig.3 (b) shows four curves of measuring sum from (19), which are globally decreasing.

Table 1 further shows the effect of the object size  $r$  to all measurements in COMSOL Multiphysics [25], where  $\kappa$  is fixed to 25%, 30%, and 40%, respectively. The change of all measurements is evaluated by their sums. For each fixed

TABLE 3. Fundamental characteristics of solid and liquid objects.

	Fine sand	Small stone	Sand–stone mixture
Solid particular			
Size $r$ (mm)	0.00234	0.02320	0.01651
$\gamma$ (uS/cm)	0.035/ 16.23/32.5	0.035/ 16.23/32.5	0.035/ 16.23/32.5

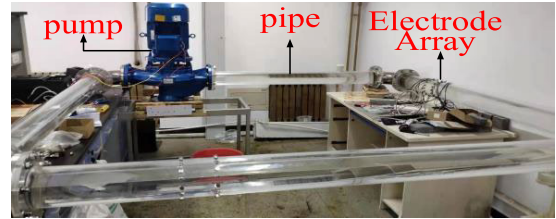


(b) Comparison between  $\phi_i^{full}$  and  $\phi_i^{ref}$   
 FIGURE 4. Determination of range of  $q$  in the proposed method.

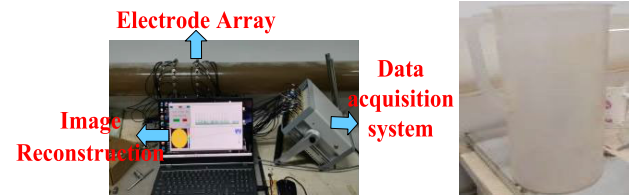
$\kappa$  the object size  $r$  is taken as a set of increasing values, but these measuring sums are very different. The curve of each measuring sum has a decreasing trend as  $r$  increases, and these curves under different values of  $\kappa$  have different distributed ranges. Therefore, their maximal difference of  $\kappa$  computed by MG attains 36% original value of  $\kappa$  along various object sizes.

B. THE COMPUTATION OF  $\kappa$

The value of  $q$  in (15) principally ranges in the interval (0, 1) but it must be determined in advance. The existing researches



(a) The layout of experiment



(b) The ERT system



(c) Measuring cylinder

FIGURE 5. Reconstructed measurements of the mixture with various sizes.

[26] has proved that the difference between  $\phi_i^{ref}$  in  $\Omega_0$  and  $\phi_i^{full}$  in  $\Omega$  is subject to

$$\phi_{i-2}^{ref} < \phi_i^{full} < \phi_{i+2}^{ref}, \quad i = 3, 4, \dots, 13 \quad (20)$$

Fig. 4(a) simulates a two-phase flowing field that consists of blue objects and red backgrounds, and (b) shows their measurements  $\phi_i^{ref}$  and  $\phi_i^{full}$ , respectively. After solving (20), the range of  $q$  can be restricted to a more accurate interval than (0, 1).

Table 2 shows a group of solutions of  $q$  according to (20) when the background conductivity  $\gamma$  is individually taken as 32.51, 18.52, and 0.055 uS/cm along a group of values of  $\kappa$ . It is seen that the solved range of  $q$  is very small, and the resultant relative error between maximal and minimal measurements is small as well. Meanwhile, Table 2 shows that the range of relative error nearly is reduced as  $\gamma$  decreases or  $\kappa$  rises.

After determining  $q$  and  $r$ ,  $\kappa$  in (18) can be solved from  $i$ th measurement  $\phi_i$  as

$$\kappa_i = \frac{\pi r}{2d_i} \log_q \left( 1 - \frac{(1-q)I - 4\pi(1-q)\gamma d_i \phi_i}{4\pi(\pi-2)\gamma r \phi_i} \right), \quad i = 1, 2, \dots, 15 \quad (21)$$

If all solid objects are evenly distributed in  $\Omega$ , the computed value  $\kappa_i$  by (21) are mutually equal among all measurements.

Then any measurement can principally determine the value of  $\kappa$ . However, there are at least the three reasons such that (21) may be inaccurate when using a single measurement:

1) It is impossible that all object sizes are consistent. Objects with various sizes may randomly appear in  $\Omega$  everywhere, which must lead to nonlinear change of the related measurements. So, these measurements will work out different values of  $\kappa$  from (21).

2) The computed value by (15) may have error compared with actual value, and the actual exciting current can depart way from the shortest way from any exciting to measuring electrodes. Meanwhile, although all currents go through the same field  $\Omega$ , but each of them may have various intensity in individual pass-by area.

3) The assumption of a decreasing geometric progression in our method may be inaccurate to some extent. Due to the existence of parasitic resistance in the voltage-driven ERT system [26], each ERT measurement are inevitably affected more or less.

To overcome the above problems, we compute  $\kappa$  using the mean of solved SPF values by (21) along all measurements in the ERT system. It is

$$\kappa = \sum_{i=1}^{240} \kappa_i / 240,$$

$$s.t., \kappa_i = \frac{\pi r}{2d_i} \log_q \left( 1 - \frac{(1-q)I - 4\pi(1-q)\gamma d_i \varphi_i}{4\pi(\pi - 2)\gamma r \varphi_i} \right) \quad (22)$$

In practice, the values of  $d_i$ ,  $\gamma$ ,  $r$  must be determined in advance. Finally, after taking all the actual measurements into (22),  $\kappa$  can be computed effectively.

Hereafter, we call the extend MG formula as EMG. The MG formula must be calibrated by (9), whereas EMG must be done by the value of  $q$ .

#### IV. EXPERIMENT

Experiments were carried out at a constructed platform. It consists of a closed square pipeline with 8000mm length and 800 mm pipe diameter. A pump in the pipe provides flowing power, whereas an ERT system obtains measurements in real time (see Fig.5 (a)). The soil/sand particles (objects) and water were filled into the pipe to generate solid-liquid two-phase flows, and flow velocity was adjustable by means of the pump. The averaging flowing velocity was 1.5–2.7 m/s, where the setting of the lower bound 1.5m/s aims to make all solid objects be under floating state. Therefore, the two-liquid flow is nearly even-distributed in any cross section in the pipe.

The ERT system with 16 electrodes and 68dB SNR is made in Tianjin University, China, which is used to collect all measurements in experiments (see Fig.5(b)),

The volume capacity of the pipeline is 82.5cm<sup>3</sup>, whereas the added solid particles and water are measured by a cylinder (see Fig.5(c)). Hence, the mean of solid phase fraction  $\kappa$  at each cross section can be computed by the rate of the cumulative particulars and water volumes.  $\kappa$  is adjusted from 0.10 to 0.25. And a floating object is putted into the two-phase flow to

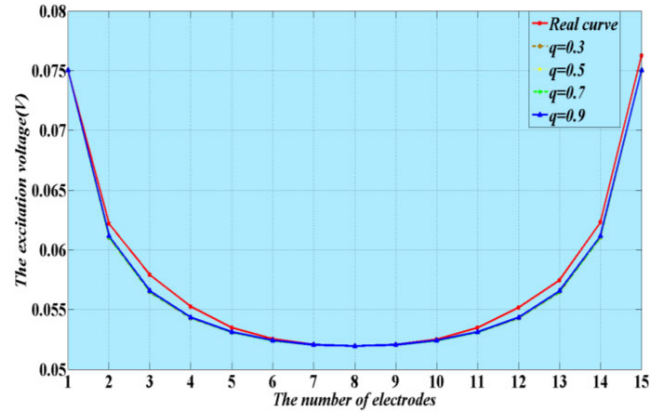
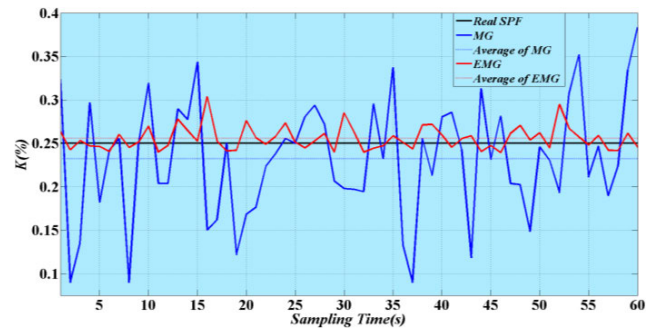
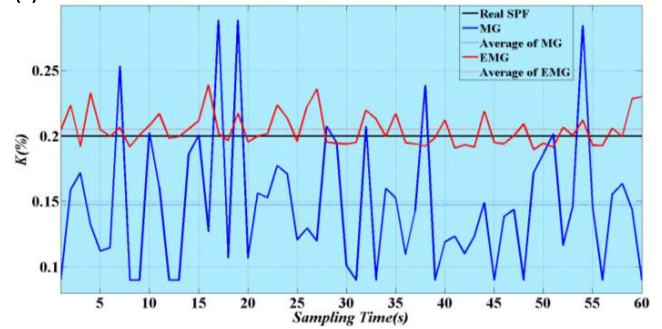


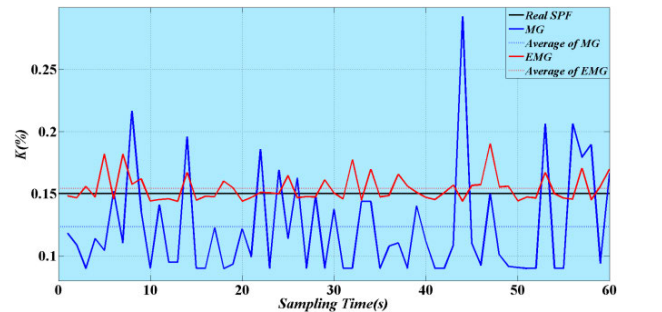
FIGURE 6. Comparison of the reconstructed and real measurements along various values of  $q$ .



(a)  $\kappa=0.25$



(b)  $\kappa=0.20$



(c)  $\kappa=0.15$

FIGURE 7. Evaluation of transient values of  $\kappa$  under the three sets of experiments.

observe and compute flowing velocity owe to the transparent pipe. The floating object-based velocity is denoted as  $FV$ .



$$\sigma_{mc}/\sigma_1 = \begin{cases} 0.003808 \sum_{j=1}^{812} \sum_{i=1}^{240} s_{ij} \Delta u_i - 0.1072, & \text{in fine sand} \\ 0.005584 \sum_{j=1}^{812} \sum_{i=1}^{240} s_{ij} \Delta u_i - 0.5908, & \text{in small stone} \\ 0.005068 \sum_{j=1}^{812} \sum_{i=1}^{240} s_{ij} \Delta u_i - 0.4717, & \text{in mixed particle} \end{cases} \quad (23)$$

TABLE 4. Comparable SPF from MG and EMG along various object sizes.

	Equation \ $\kappa$	0.15	0.2	0.25	0.3	0.35
	Fine sand ( $r=0.00234$ mm)	MG	0.1162	0.1299	0.2250	0.2692
EMG		0.1499	0.2050	0.2555	0.3020	0.3445
Small stone ( $r=0.02320$ mm)	MG	0.1726	0.2011	0.2074	0.2854	0.3381
	EMG	0.1500	0.2043	0.2556	0.3040	0.3493
Sand-stone mixture ( $r=0.01651$ mm)	MG	0.1624	0.1785	0.2124	0.2851	0.3245
	EMG	0.1499	0.2020	0.2514	0.2986	0.3436

And thus,  $FV$  is accurate and reliable although it cannot reflect transient velocity at each cross section. When the solid-liquid two-phase fluid at  $l$ th experiment attains a steady flow state, the mean of  $\kappa$  along all sampling times must be a constant, denoted it as  $K(l)$ ,  $l = 1, 2, \dots, L$ . The transient value of  $\kappa$  must be change around  $K(l)$ . If the value of  $EMG$  or  $MG$  is accurate, their mean must be equal to  $K(l)$ ,  $l = 1, \dots, L$ .

Three kinds of solid particles are used including fine sand, small stone, and sand-stone mixture, respectively. Their conductivities are nearly zero but have individual averaging radius 0.00234, 0.0232, and 0.0165 cm. After adding salt to water, its conductivity is modulated to 0.035, 16.0, and 32.5  $\mu S/cm$ , respectively. Table 3 shows the fundamental characteristics of solid and liquid (water) objects in the experiments.

According to the above characteristics, the accuracy and applicable range of  $EMG$  are evaluated compared with  $MG$  under three sets of experiments.

To compute  $\kappa$  by  $MG$ , the relation between  $\sigma_{mc}$  and  $u$  in (9) is required to determine after salt water of  $\gamma$  is taken individually as 0.035, 16.0, and 32.5  $\mu S/cm$ . According to the three sets of sampling measurements on pairs  $(\sigma_{mc}, u)$ , the necessary relation is solved as (23), shown at the top of the page.

In term of the same measurements,  $q$  in (22) is determined along the above three groups of fundamental characteristics. Fig.6 shows that three curves that consist of computed measurements under different values of  $q$  when  $\gamma=32.5 \mu S/cm$ ,  $r = 0.00234$ . It is seen that the reconstructed measurements are very consistent to the actual ones in a wide range of  $q$ . In the following experiments, we uniformly fix  $q$  to 0.90.

Table 4 shows that the computed mean of  $\kappa$  by  $EMG$  is more consistent with the actual ones than that by  $MG$  at the three sets. Larger size the objects have and larger error  $MG$  has. We thus conclude that  $MG$  only is effective when  $r$  tends to small enough, and else is erroneous very much. These results recover the reason why  $MG$  is inaccurate under larger size, but the difference between  $MG$  and  $EMG$  becomes small as  $r$  decreases.

With a close look on the accuracy of (22) along various sizes of  $r$ , Fig.7 shows that computed transient values of  $\kappa$  by  $MG$  and  $EMG$  when  $\kappa(l)=0.15, 0.20$ , and  $0.25$ , respectively. The mean of  $EMG$  is closer to the value of  $\kappa(l)$  than that of  $MG$ . And Each  $EMG$  curve fluctuates around the corresponding line of  $\kappa(l)$ , whereas  $MG$  does not fluctuate along the line. Meanwhile, the amplitude of the computed values using  $EMG$  is much smaller than that of  $MG$ . Therefore,  $EMG$  is more accurate no matter which object size is encountered. However, when the applicable condition of  $EMG$  is not meet, it must include errors. There are inevitable noisy measurements in an ERT process, leading to the error between the computed values of  $\kappa$  and the actual ones.

In summary, the above experimental results demonstrate that  $EMG$  can provide higher accuracy to compute  $\kappa$  along various object sizes if its applicable condition is meet.

## V. CONCLUSION

The current  $SPF$  estimation methods based on  $ERT$  are problematic in solid-liquid two-phase flow since these methods have three inevitable limitations. Our proposed method can decrease the negative effect of these limitations. To our knowledge, so far there is none formulas that can effectively compute  $SPF$  along various object sizes. The preliminary results presented in this paper show that the proposed method is comprehensive and effective for estimating the  $SPF$  values.

But the proposed method in this paper sometime is uncomplete and inaccurate under complex flow conditions, such as changeable liquid conductivity and uneven objects distributions in cross-section in a pipe. Meanwhile, the mean of object size is necessarily known in prior. To overcome these problems is just the work we are focusing on in present.

## REFERENCES

- [1] Z. M. Wang, B. M. Li, J. Z. Li, H. Y. Wang, and J. T. Li, "Sand movement by heavy oil in a horizontal wellbore," *Energy Sour. A, Recovery, Utilization, Environ. Effects*, vol. 37, no. 6, pp. 655–662, Mar. 2015.
- [2] L. Yenumula, R. V. Acharya, U. Kumar, T. P. Selvam, K. Roy, V. H. Patankar, and S. Kar, "Ring artifact correction in gamma-ray process tomography imaging," *Appl. Radiat. Isot.*, vol. 124, pp. 75–82, Jun. 2017.



- [3] Y. Xu, Q. Wang, X. Jiang, H. Zu, W. Wang, and R. Feng, "Nondestructive assessment of microcracks detection in cementitious materials based on nonlinear ultrasonic modulation technique," *Construct. Building Mater.*, vol. 267, Jan. 2021, Art. no. 121653.
- [4] Z. Wang, S. Yue, X. Liu, A. McEwan, B. Sun, and H. Wang, "Estimating homogeneous reference frame for absolute electrical impedance tomography through measurements and scale feature," *IEEE Trans. Instrum. Meas.*, vol. 70, pp. 1–12, 2021.
- [5] Z. Wang, S. Yue, Q. Li, and H. Wang, "Application of mirror image method in EIT to detect lung lesions," *Basic Clinical Pharmacol. Toxicol.*, vol. 1274, p. 28, Sep. 2020.
- [6] R. Wang, L. Miao, and Y. Ma, "A reference conductivity fitting method for ERT system to achieve void fraction of gas/liquid flow," *Flow Meas. Instrum.*, vol. 40, pp. 206–215, Dec. 2014.
- [7] I. V. Andrianov, J. Awrejcewicz, and G. A. Starushenko, "Asymptotic analysis of the Maxwell Garnett formula using the two-phase composite model," *Int. J. Appl. Mech.*, vol. 7, no. 2, Apr. 2015, Art. no. 1550025.
- [8] Y. Cheng, N. Zhao, K. Zhang, and W. Wei, "Research on the plume stability of air bubble curtains under low transverse flow velocity environment in dredging engineering," *Ocean Eng.*, vol. 232, Jul. 2021, Art. no. 109133.
- [9] J. Jia, M. Wang, and Y. Faraj, "Evaluation of EIT systems and algorithms for handling full void fraction range in two-phase flow measurement," *Meas. Sci. Technol.*, vol. 26, no. 1, Jan. 2015, Art. no. 015305.
- [10] M. A. Lewis, D. E. Weber, R. S. Stanley, and J. C. Moore, "Dredging impact on an urbanized Florida bayou: Effects on benthos and algal-periphyton," *Environ. Pollution*, vol. 115, pp. 161–171, Oct. 2001.
- [11] H. Jin, Y. Lian, S. Yang, G. He, and Z. Guo, "The parameters measurement of air–water two phase flow using the electrical resistance tomography (ERT) technique in a bubble column," *Flow Meas. Instrum.*, vol. 31, pp. 55–60, Jun. 2013.
- [12] A. Mohammadpour, M. A. Akhavan-Behabadi, M. Ebrahimzadeh, P. Hanafizadeh, and M. Raisee, "Experimental determination of void fraction in surface aeration using image processing technique," *J. Mech. Sci. Technol.*, vol. 29, pp. 2391–2400, Sep. 2015.
- [13] L. Xiao, Q. Xue, and H. Wang, "Finite element mesh optimisation for improvement of the sensitivity matrix in electrical resistance tomography," *IET Sci. Meas. Technol.*, vol. 9, pp. 792–799, Sep. 2015.
- [14] F. Hernandez-Alvarado, S. Kleinbart, D. V. Kalaga, S. Banerjee, J. B. Joshi, and M. Kawaji, "Comparison of void fraction measurements using different techniques in two-phase flow bubble column reactors," *Int. J. Multiphase Flow*, vol. 102, pp. 119–129, May 2018.
- [15] A. Boyle, P. B. Wilkinson, J. E. Chambers, P. I. Meldrum, S. Uhlemann, and A. Adler, "Jointly reconstructing ground motion and resistivity for ERT-based slope stability monitoring," *Geophys. J. Int.*, vol. 212, no. 2, pp. 1167–1182, Feb. 2018.
- [16] F. Fabrizio, *A Primer on Electromagnetic Fields*. Cham, Switzerland: Springer, 2015.
- [17] B. Sun, S. Yue, Z. Cui, and H. Wang, "A new linear back projection algorithm to electrical tomography based on measuring data decomposition," *Meas. Sci. Technol.*, vol. 26, no. 12, Dec. 2015, Art. no. 125402.
- [18] M. Ding, S. Yue, J. Li, Y. Wang, and H. Wang, "Second-order sensitivity coefficient based electrical tomography imaging," *Chem. Eng. Sci.*, vol. 199, pp. 40–49, May 2019.
- [19] F. Santosa and M. Vogelius, "A backprojection algorithm for electrical impedance imaging," *SIAM J. Appl. Math.*, vol. 50, pp. 216–243, Feb. 1990.
- [20] M. Vauhkonen, D. Vadasz, P. A. Karjalainen, E. Somersalo, and J. P. Kaipio, "Tikhonov regularization and prior information in electrical impedance tomography," *IEEE Trans. Med. Imag.*, vol. 17, no. 2, pp. 285–293, Apr. 1998.
- [21] N. Tarabi, H. Mousazadeh, A. Jafari, J. Taghizadeh-Tameh, and A. Kiapay, "Developing and evaluation of an electrical impedance tomography system for measuring solid volumetric concentration in dredging scale," *Flow Meas. Instrum.*, vol. 80, Aug. 2021, Art. no. 101986.
- [22] Z. Cui, Q. Wang, Q. Xue, W. Fan, L. Zhang, Z. Cao, B. Sun, H. Wang, and W. Yang, "A review on image reconstruction algorithms for electrical capacitance/resistance tomography," *Sensor Rev.*, vol. 36, pp. 429–445, Sep. 2016.
- [23] Z. Cui, C. Yang, B. Sun, and H. Wang, "Liquid film thickness estimation using electrical capacitance tomography," *Meas. Sci. Rev.*, vol. 14, no. 1, pp. 8–15, Feb. 2014.
- [24] P. Heering, J. Keck, and G. A. Rohlfs, "Laboratory notes, laboratory experiences, and conceptual analysis: Understanding the making of Ohm's first law in electricity," *Berichte Wissenschaftsgeschichte*, vol. 43, no. 1, pp. 7–27, Mar. 2020.
- [25] Z. Wang, S. Yue, Q. Li, X. Liu, H. Wang, and A. McEwan, "Unsupervised evaluation and optimization for electrical impedance tomography," *IEEE Trans. Instrum. Meas.*, vol. 70, pp. 1–12, 2021.
- [26] Z. Wang, S. Yue, H. Wang, and Y. Wang, "Data preprocessing methods for electrical impedance tomography: A review," *Physiol. Meas.*, vol. 41, Oct. 2020, Art. no. 09TR02.



**YONGGUANG TAN** received the B.S. and M.S. degrees from the Xi'an University of Architecture and Technology, Shanxi, China, in 2014 and 2018, respectively. He is currently pursuing the Ph.D. degree with Tianjin University. His research interests include electrical tomography image reconstruction and data mining.



**SHIHONG YUE** received the M.S. and Ph.D. degrees in application mathematics from the Xi'an University of Technology, Shanxi, China, in 1997 and 2000, respectively.

He is currently a Professor at the School of Electrical and Information Engineering, Tianjin University, China. His current research interests include process parameter detection, medical image processing, data mining, and intelligent instrumentations.



**ZIQIANG CUI** (Member, IEEE) received the M.Sc. and Ph.D. degrees from Tianjin University, Tianjin, China, in 2007 and 2009, respectively.

He is currently an Associate Professor with the School of Electrical and Information Engineering, Tianjin University. His current research interests include electrical tomography instrumentation, signal processing, sensor design, and multiphase flow measurement.



**HUAXIANG WANG** (Senior Member, IEEE) received the M.S. degree in measurement technology and automatic devices from Tianjin University, Tianjin, China, in 1982.

He has authored five books and over 100 academic papers. His major research projects and activities are in the areas of sensing techniques and information processing, process parameter detection and control systems, and intelligent instrumentation systems.

...